Numerical analysis of the behaviour of vessels advancing through restricted shallow waters

Tahsin Tezdogan[1], Momchil Terziev, Elif Oguz, Atilla Incecik

Department of Naval Architecture, Ocean and Marine Engineering, Henry Dyer Building,

University of Strathclyde, 100 Montrose Street, Glasgow, G4 0LZ, UK

[1]*Corresponding author;* e-mail: tahsin.tezdogan@strath.ac.uk, phone: +44(0)1415484532

ABSTRACT

Upon entering shallow waters, ships experience a number of changes due to the hydrodynamic interaction between the hull and the seabed. Some of these changes are expressed in a pronounced increase in sinkage, trim and resistance. In this paper, a numerical study is performed on the Duisburg Test Case (DTC) container ship using Computational Fluid Dynamics (CFD), the Slender-Body theory and various empirical methods. A parametric comparison of the behaviour and performance estimation techniques in shallow waters for varying channel cross-sections and ship speeds is performed. The main objective of this research is to quantify the effect a step in the channel topography on ship sinkage, trim and resistance. Significant differences are shown in the computed parameters for the DTC advancing through dredged channels and conventional shallow water topographies. The different techniques employed show good agreement, especially in the low speed range.

Keywords*:* Ship squat; Slender Body Theory; CFD; ship resistance; trim and sinkage

1. Introduction

Ship behaviour and performance are highly influenced by the hydrodynamic interaction between the hull and the proximity of the seabed. Namely, the flow velocity between the hull's bottom and the seabed increases, which produces a drop in pressure. This can be thought of in terms of the Bernoulli principle, where an increase in kinetic energy causes a decrease in pressure in order to satisfy the energy conservation condition (Debaillon, 2010). The abovementioned pressure reduction creates a vertical downward force and moment about the ship's transverse axis, leading to an increase in sinkage coupled with trim (known as squat), and resistance.

In order to accurately assess the ship's power requirements, it is important to understand the resistance a vessel would encounter throughout its operational life. According to some authors, ships experience a drop in speed of up to 30% upon entering shallow waters (Tezdogan et al., 2016). This value can rise up to 60% when operating in rivers or canals (Barrass, 2012). Beck et al. (1975) investigated both a channel with the presence of a depth discontinuity (dredged channel) and a vertical-walled canal. They found that

the water surrounding the depth discontinuity in a dredged canal configuration can affect the computed results significantly.

The literature offers a wealth of techniques to calculate the squat and trim of a ship in restricted waterways. These include empirical formulations, analytical, experimental and numerical methods. The empirical formulations can give substantially different values when applied to the same case-study. Analytical methods use slender-body theory and the assumptions inherent of this approach. Experimental methods can be expensive and highly dependent on the schedule and availability of testing facilities. On the other hand, computational fluid dynamics (CFD) techniques have been shown to be capable of accurately predicting the sinkage, trim and resistance of vessels in shallow waters. Moreover, this can be done while accounting for viscous effects as well as non-linear terms.

For the abovementioned reasons, the current study aims to conduct an in-depth parametric analysis and prediction of the resistance, trim and sinkage of a vessel advancing through a channel with varying underwater topographies. In this respect, the Slenderflow code is used in this study. The code has been devised employing the Slender-Body theory developed by Tuck (1966) for shallow open water, Tuck (1967) for canals, and later expounded upon by Beck et al. (1975) to incorporate dredged channels. The empirical formulations compiled by PIANC (1997) and Briggs (2006), (2009) are also coded into a separate MATLAB code for comparison. A commercial CFD package was utilised to carry out unsteady Reynolds Averaged Navier-Stokes (RANS) simulations on the Duisburg Test Case (DTC) containership for varying speeds and channel geometries. For each simulation, the trim, and sinkage time-histories were recorded at the vessels centre of gravity (CoG) as well as the drag shear and pressure forces time-history. For the purposes of this study, Star-CCM+, version 11.02, developed by CD-Adapco was used.

2. Background

This section is organised in accordance to the squat evaluation methods. Background on the analytical method employed in this paper is given first.

2.1 Analytical methods

Interest in the field of shallow water hydrodynamics can be traced back to the famous paper by Michell (1898). In his publication, he devised a thin-body method to predict the wave resistance of a ship moving in shallow water. The fundamental assumption behind the Michell (1898) method is that the ship's beam is small compared to its length. As a consequence of this, the waves generated are also of small amplitude, which allows the linearisation of the free water surface.

Havelock (1908) investigated the wave pattern created by the propagation of a point source in shallow water. His work led to the introduction of the non-dimensional depth Froude number (F_d)

$$F_d = \frac{V}{\sqrt{gh}} \tag{1}$$

Where V is the vessel's speed, g is the acceleration due to gravity ($g = 9.81 \ m/s$) and h is the water depth. The depth Froude number can be thought of as the ratio of the ship's speed to the maximum wave

velocity in shallow water of depth h. The terms subcritical and supercritical speed are used for vessels propagating at $F_d < 1$ and $F_d > 1$, respectively. Of greater practical interest is the former scenario, namely when the depth Froude number is smaller than 1 (Beck et al., 1975).

Tuck (1966) reproduced Michell's linearised Slender-body theory, and solved for the hydrodynamic forces in shallow water. In his paper, Tuck (1966) explored the scenario where a ship is travelling in shallow waters of constant infinite width. He used the vertical forces and moments acting on the ship to successfully compute the sinkage and trim for sub- and supercritical speeds, and validated the results with model-scale experiments. With regards to resistance, the method developed by Tuck (1966) predicts zero resistance in the subcritical range.

Later, Tuck (1967) investigated the effect of restricted channel width as well as depth on ship behaviour. Beck et al. (1975) expanded on the previously mentioned work to account for vessels in dredged canals (**Error! Reference source not found.**) with an infinite shallow water region of constant depth (h_∞) extending on either side of the dredged section on the channel (of depth h_0).

1.3 Reynolds Averaged Navier-Stokes (RANS) based numerical techniques

In this section, the relevant Computational Fluid Dynamics (CFD) contribution to the field of shallow water hydrodynamics briefly touched upon.

Jachowski (2008) employed a commercially available RANS based numerical software package to predict ship squat in shallow waters. He applied this technique to the KRISO Containership (KCS) model. The results were compared to those calculated by empirical formulations and good agreement was found between the two methods

Wortley (2013) performed a CFD investigation of the sinkage and trim on the DTC containership in OpenFOAM, an alternative RANS solver. Wortley (2013) used two different software to compare his results. He reported that as a consequence of the insufficient resolution of the generated mesh, the wave resistance is overestimated.

Mucha and el Moctar (2014) performed numerical analyses using potential flow and RANS methods and compared their results for sinkage, trim and resistance to available experimental data for the KCS model in shallow water. More recently, Tezdogan et al. (2016) investigated the performance and behaviour of the DTC in an asymmetric canal as part of the Pre-Squat workshop initiated by the University of Duisburg-Essen (further information can be found in Mucha et al., 2014). To perform their analysis, Tezdogan et al. (2016) employed CD-Adapco's Star-CCM+ RANS solver and showed that the results obtained in model scale are in good agreement with experimental results.

In the present paper, the same vessel as the one used by Tezdogan et al. (2016) is used and the numerical setup is the same except the canal geometry. In Tezdogan et al. (2016)'s study an asymmetric canal geometry was modelled as adopted from Mucha et al. (2014). Therefore the study reported in this paper heavily relies on the CFD modelling described in Tezdogan et al. (2016), which is already verified and validated against experimental work of Uliczka (2010).

3. Ship hull and channel geometry

The DTC model, whose 3-D CAD (Computer-Aided Design) hull, propeller and rudder data are all readily available in the public domain, were developed by the University of Duisburg-Essen benchmarking purposes. This hull form was designed to be utilised as a model for numerous investigations, and various authors have made use of the DTC to conduct research (el Moctar et al., 2012).

Figure 1. 3D geometry of the DTC; modelled in Star-CCM+ (Tezdogan et al., 2016).

A scale factor of 1:40 was chosen to match the experiments performed on this ship in other studies. The 3D model of the DTC as modelled in Star-CCM+ in shown in Figure 1. As part of the initial conditions, an even-keel draught, with full-scale equivalent of 14.5 m was set throughout the case-studies performed in this paper. The main particulars and other relevant information can be found in (el Moctar et al., 2012). Since the research idea behind this paper was to investigate the effect of the presence of a step in the channel, it is evident that this scenario will be focused upon. Beck et al. (1975) place great emphasis on the height of the step in proportion to the overall depth. In this study, the abovementioned ratio (h_∞/h_0) was varied between 1 and 0 at three equal intervals for each depth Froude number, as shown in Table 1. The width of the inner region was chosen based on the results detailed by Beck et al. (1975). By reviewing the graphs produced by Beck et al. (1975), it became evident that when the inner width to ship length ratio is equal to 0.5 the effect of the step is amplified. Therefore, this configuration was selected to investigate the influence of the depth discontinuity as this assumption is likely to produce the most palpable differences between configurations. According to the ITTC's CFD guidelines, any boundary should be placed between 1 and 2 ship lengths away from the vessel (ITTC, 2011). To minimise the computational effort, the lateral boundaries were placed at a distance of 1 ship length away from the step on each side. This amounts to 1.25 ship lengths distance between the vessel's centreline and the transverse boundaries on each side of the ship, as depicted in Figure 2.

Table 1. Channel configurations.

Case-study	Ratio	Ratio Value	Step Height (m)
Channel 1	h_∞/h_0	1	0
Channel 2	h_∞/h_0	0.33	0.311
Channel 3	h_∞/h_0	0.66	0.155
Channel 4	h_∞/h_0	0	0.471

The case-studies detailed in Table 1 are used in both the Slender-Body theory and CFD runs. To compare the performance of these two different methods more accurately, each case-study is run for different speeds. The channel cross-sections are shown in Figure 2.
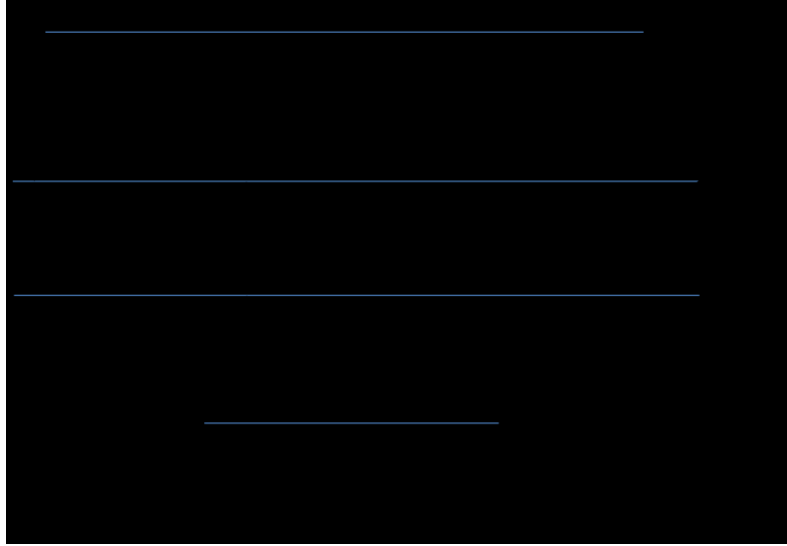

Figure 2. Channel cross-sections, not to scale.

4. Numerical Modelling

In this section, the numerical modelling techniques will be discussed in detail. As stated previously, the numerical setup employed in this paper is similar to that explained in detail in Tezdogan et al. (2016). For further details, the reader can refer to Terziev et al. (2018)

4.1 Physics modelling

To model the turbulence in the fluid, a standard $k - \varepsilon$ model was employed with the all y^+ wall treatment, which has been widely used in similar studies Tezdogan et al. (2015), Tezdogan et al. (2016). To characterise the free surface, the volume of fluid (VOF) method was adopted to model and position the boundary between phases. The concept of a flat wave is used to represent the movement of water particles relative to the ship hull in the context of this paper. The water surface is free to move, depending on the disturbance caused by the presence of the ship. An increased mesh resolution is imposed in the region where the free surface is expected to undergo sharp local gradients i.e. the formation of waves. The convection terms in the Navier-Stokes equations are discretised using a second order upwind scheme. This was done to avoid the smearing of the free surface, which would likely happen if a lower order scheme had been adopted instead (CD-Adapco, 2016).

A segregated flow model was utilised to solve the governing Navier-Stokes equations in an uncoupled manner. To solve these equations, the Semi-Implicit Method for Pressure Linked Equations (SIMPLE) algorithm was utilised. In order to ensure the accurate representation of ship motions, Star-CCM+ offers a Dynamic Fluid-Body Interaction (DFBI) module.

To control the time step, the Implicit Unsteady option of Star-CCM+ was selected. In a similar study, where the DTC's sinkage and resistance in shallow waters were analysed, a time-step convergence study was carried out, which suggested that the time step should equal 0.0035L/V. Finally, the temporal discretisation was set as first order to discretise the time variant term in the governing Navier-Stokes equation.

4.2 Computational Domain

The width of the domain in Beck et al. (1975) is infinite, however, doing this in Star-CCM+, or in fact in any CFD software is not possible, therefore, the transverse boundaries have been placed suitably. CD-Adapco (2016), recommends that the velocity inlet of the computational domain for resistance prediction should be located at least one ship length upstream from the forward perpendicular, and the pressure outlet at least twice that distance downstream, from the respective perpendicular. To conform to these recommendations, the inlet boundary was set $1.22L$ ahead of the forward perpendicular and the pressure outlet $2.23L$ downstream from the aft perpendicular (CD-Adapco, 2016, Tezdogan et al., 2016). To eliminate the possibility of a wave reflection from these boundaries, a VOF wave damping option was enforced, the length of which was set as to equal $1.127L \approx 10m$ used in both longitudinal and transverse directions.

The boundary in the positive x-direction was set as a velocity inlet, where the flat wave originates, and the negative x-direction was set as pressure outlet, which prevents backflow and fixes static pressure at the outlet. To allow the simulation to resemble real life towing tank experiments as close as possible, the domain top was placed $1.127L \approx 10m$ away from the still waterline, where the Newman boundary condition was applied. Next, the virtual towing tank bottom is set as a 'wall' which employs the built-in (non-slip) function of Star-CCM+ describing this phenomenon. Thus, we have dealt with the domain bottom, sides and hull. Thus, the computational domain is assembled and shown graphically in
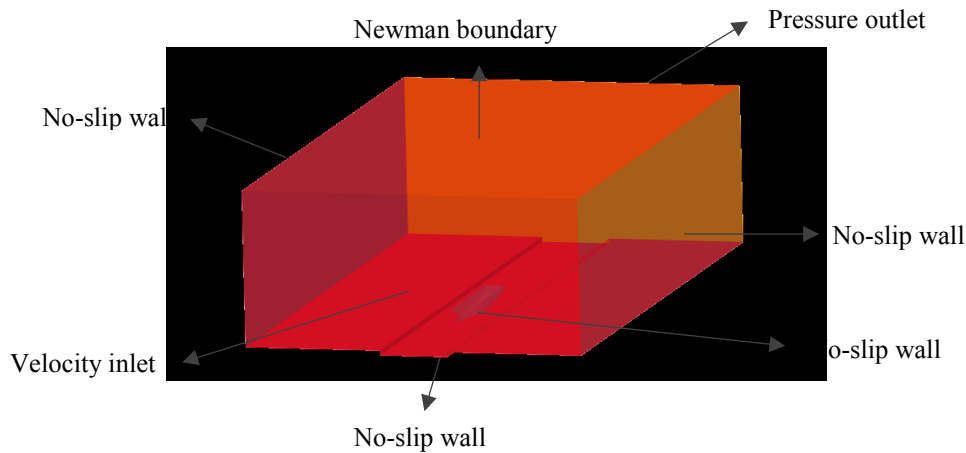
Figure **3** for channel 2.

Figure 3. Representative domain boundaries; Depicted: Channel 2 ($h_\infty/h_0 = 0.33$)

4.3 Mesh generation

Mesh generation was carried out in the facilities offered by Star-CCM+. This allows the user to make full use of the software's automatic operations. Firstly, the region-based mesh generated is static in relation to the local coordinate system and therefore to the hull. Since the DTC's appendages describe complex geometries (rudder, propeller), a high-quality trimmed cell mesher was utilised, which generated cells in the computational domain.

The Prism Layer mesher was utilised to generate orthogonal prismatic cells next to the hull. This kind of layer mesh allows the software to resolve the near-wall flow accurately as well as capture the effects of flow separation (CD-Adapco, 2016). Resolving these parameters in sufficient detail depends on the flow velocity gradients normal to the wall, which are much steeper in the viscous turbulent boundary layer than would be implied by taking gradients from a coarse mesh. Prism layer numbers were selected to ensure that the y^+ value on the ship is maintained at a value lower than 1 in order to use the low-Re y^+ treatment.
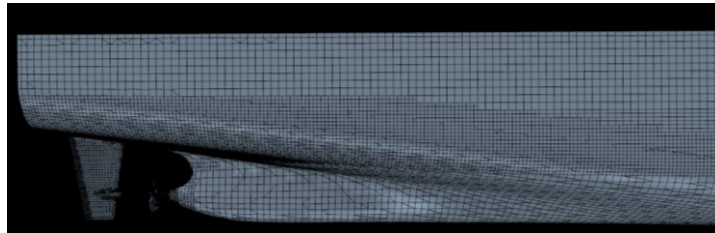

Figure 4. DTC stern mesh

A trimmed mesher option was selected, which is an efficient method of fabricating a high-quality grid for complex mesh generation. The cells created by the trimmed mesher are predominantly hexahedral and have a minimal cell skewness. Figure 4 shows the surface mesh on the hull with a focus on the stern of the ship. The wake field behind the vessel also has a refined grid density to capture the complex flow properties (Figure 5).
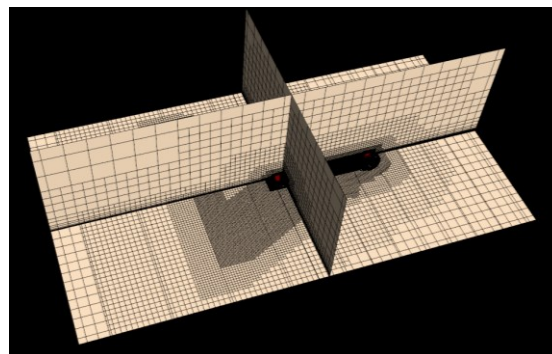

Figure 5. 3-D view of the mesh. Depicted: Channel 3 ($h_\infty/h_0 = 0.66$)

5. Results and discussion

To begin with, perhaps the most interesting and most studied variable is analysed, namely, the squat. However, in order to obtain a full picture of the ship behaviour in shallow water, the trim the vessel experiences, considered an indispensable part in the overall ship assessment, is given for each case-study. The trim is given in radians, as the Slender-Body theory output uses this unit.

5.1 Ship behaviour

5.1.1   Channel 1

For this case-study, an attempt was made to approximate the scenario of a ship advancing through unrestricted shallow water. The theory developed by Tuck (1966) describes this case-study, which has been shown to provide satisfactory results when compared to experimental data for low speeds. To perform the calculations, the Slenderflow code, which is validated in (Ha and Gourlay, 2017) was used to provide results for all configurations investigated in order to ensure that the results are accurate. The empirical formulations for unrestricted waters were employed in the in-house code. The applicable formulae and the results computed using this method up to $F_d = 0.9$ are shown in Figure 6.
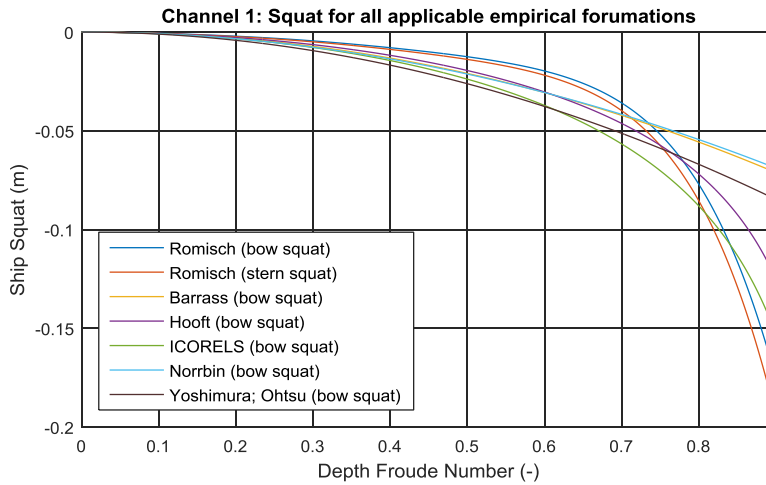

Figure 6. In-house code output: Empirical formulae for channel 1

To retain consistency, the values computed via the Slender-Body theory and CFD are presented in a together, as both methods calculate the sinkage amidships, rather than at the extremity of the vessel, which can be highly influenced by the trim. The results comparison is shown in
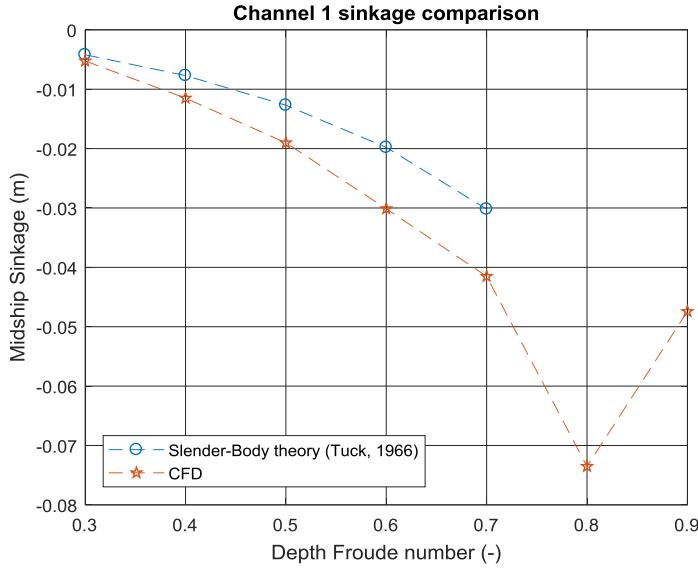
Figure 7 and Figure 8.

Figure 7. CFD and Slender-Body theory comparison for channel 1.
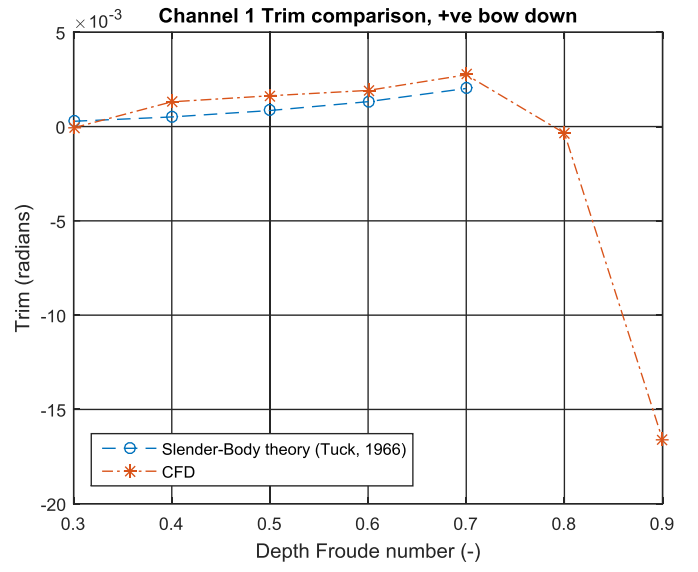

Figure 8. Dynamic trim comparison for Channel 1; positive bow down.

The results using the theory developed by Tuck (1966) are continued up to and including $F_0 = 0.7$ because non-linear and viscous effects become more important as we progress through the speed range. A slight underestimation of the CFD results can be observed throughout the velocities investigated, which is a consequence neglect of non-linear and viscous terms (Gourlay, 2008). As expected, the difference between the two sets of data gradually increases as the depth Froude number increases. Finally, the trim comparison for this case-study is presented.

Figure 8 reveals results, similar to those obtained by Gourlay et al. (2015). To elaborate, the DTC trims by bow up to $F_0 = 0.7$, which is the upper limit investigated in the abovementioned work. The experimental results for the DTC both in a rectangular and non-rectangular canal, as in Tezdogan et al. (2016), agree that the vessel squats by stern. The novel information presented here is that the DTC rapidly changes the trim mode to stern as the velocity increases past $F_0 = 0.7$.

5.1.2   Channel 2

For the two dredged channels (channel 2- $h_\infty/h_0 = 0.33$ and channel 3- $h_\infty/h_0 = 0.66$), only the empirical formulations which retain their validity for restricted configurations are applicable, as shown in Figure 9. The results computed via the Slender-Body theory for dredged channels and CFD are shown in Figure **10** and Figure 11.
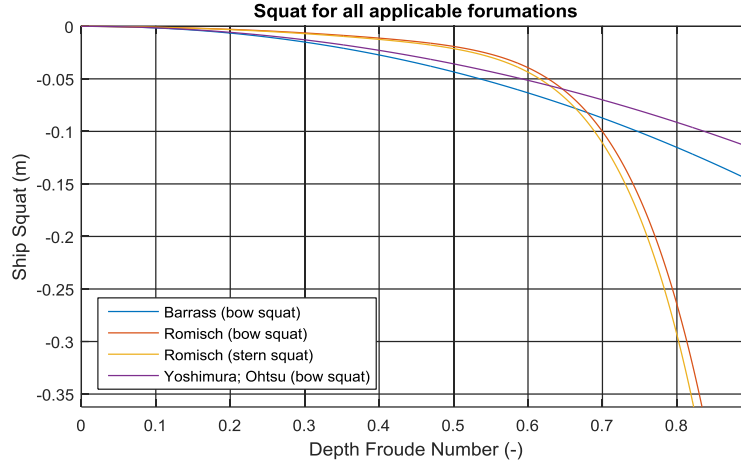
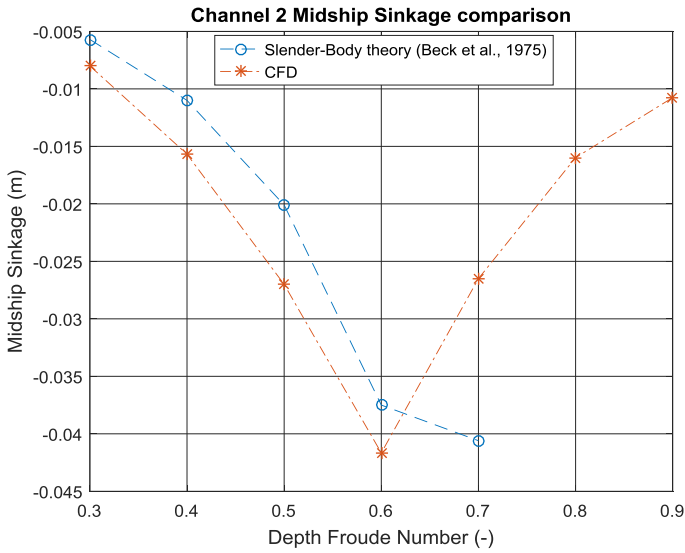**Figure 9.** In-house code output: Empirical formulae for channel 2

Figure 10. CFD and Slender-Body theory comparison for channel 2
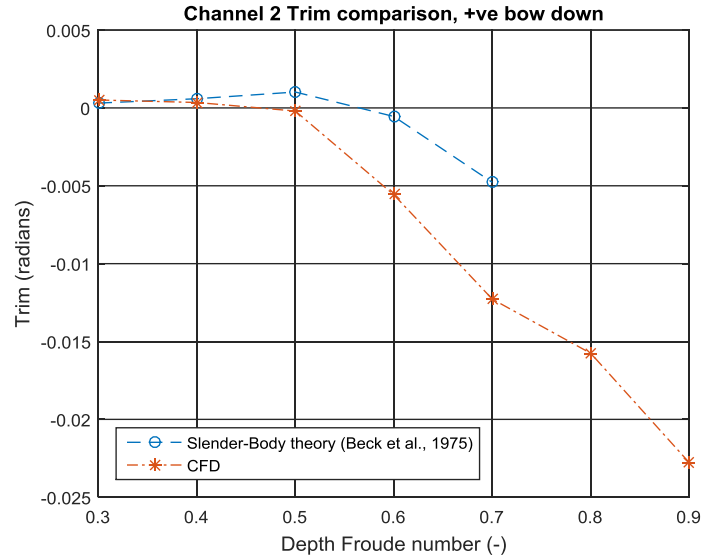

Figure 11. Dynamic trim comparison for Channel 2; positive bow down

The results for this case-study are of particular interest due to the exterior flow becoming supercritical ($F_\infty \to 1$) as $F_0 \to 0.6$. As before, the Slender-Body theory under predicts the CFD values throughout the majority of the range investigated due to the absence of non-linear and viscous terms in the theory. Similarly to the first case-study, the sinkage decreases in magnitude as the critical range is approached, as forecasted by Tuck (1966). In the present case-study, the sinkage curve slope is rapidly inverted after $F_0 = 0.6$. Comparing the trend exhibited by the sinkage values for channel 1 and the current case-study reveals the significant influence of the exterior dredged section.

In Figure 11, the Slender-Body theory and CFD results seem to agree more in the low speed range when compared to channel 1, while the values computed for $F_0 = 0.6$ and $F_0 = 0.7$ do not follow this trend. This is most likely due to the exterior flow becoming supercritical at approximately $F_0 = 0.6$. The trim

experienced by the DTC in the low speed range is significantly smaller, and changes from trim by bow to by stern much earlier than previously observed.

5.1.3   Channel 3

In this section, a case-study with a relatively deep exterior shallow water region ($h_\infty/h_0 = 0.66$) is presented. The applicable empirical formulae retaining their validity are the same as those shown in the previous section for channel 2, as shown in Figure 12.
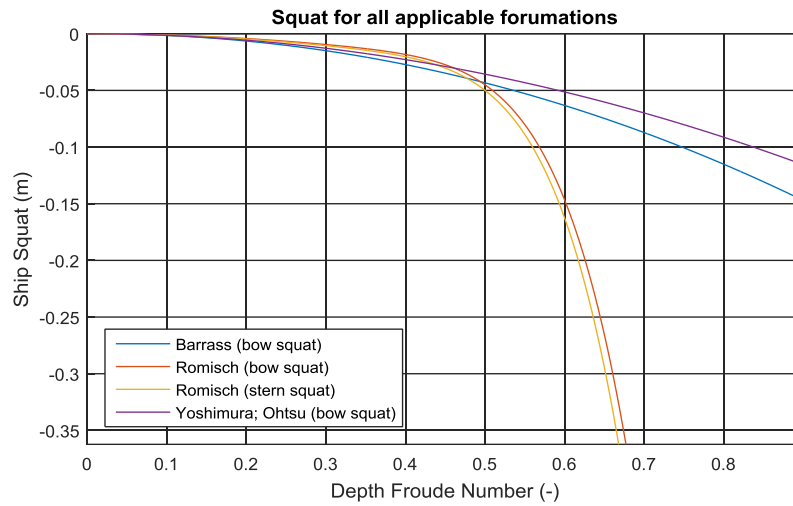

Figure 12. In-house code output: Empirical formulae for channel 3

The midship sinkage comparison between the Slender-Body theory and CFD is shown in Figure 13. The theory of Beck et al. (1975) behaves in a similar fashion as was the case for channel 2. The CFD results are underpredicted throughout the investigated velocity range, however, the difference seems to increase more in proportion as we progress towards the critical speed. This is likely since viscous and non-linear terms attain a higher relative importance than was the case for channel 2. The typical decrease in sinkage magnitude is observed as the velocity in increased. The trim comparison between CFD and the Slender-Body theory, for channel 3 is shown in Figure 14.
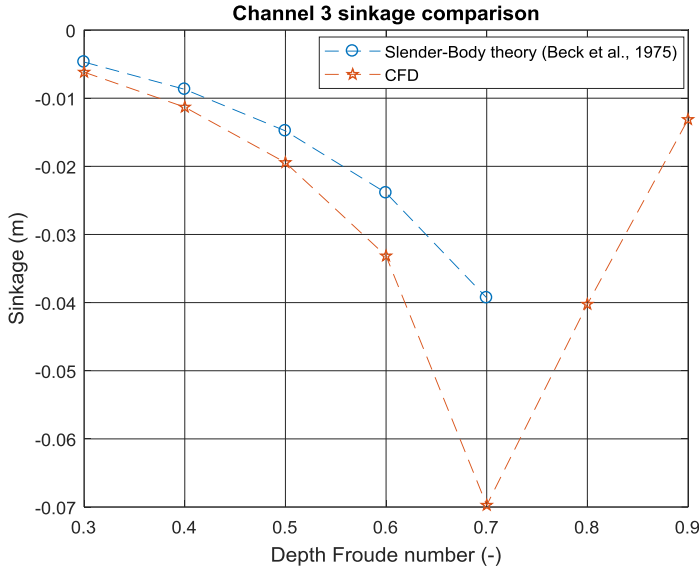
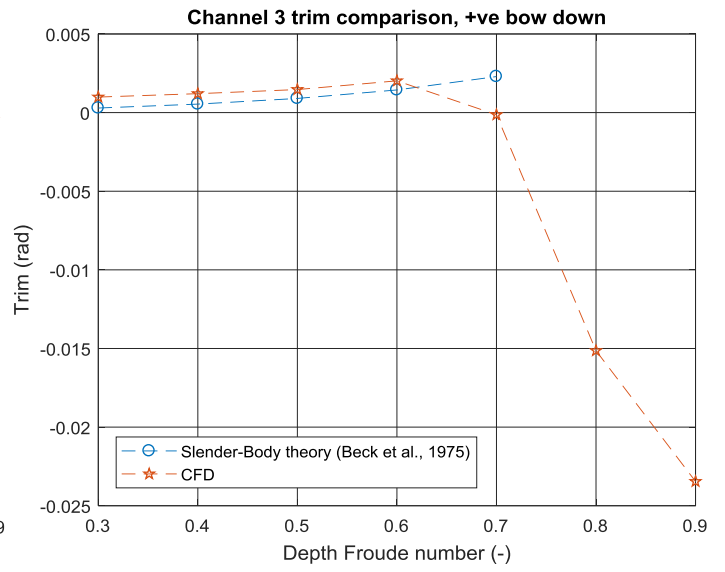**Figure 13.** CFD and Slender-Body theory comparison for channel 3

Figure 14. Dynamic trim comparison for channel 3; positive bow down

A similar trend is observed as for the previous case study in Figure 14. Namely, the trim distribution increases in magnitude as the velocity is increased. Furthermore, the two sets of data agree remarkably well in the low speed range. As the exterior flow becomes critical (at $F_0 \approx 0.8$), the trim begins to exhibit significant increase in amplitude. Channel 3 also confirms the increase in relative importance of trim angles for high speeds in shallow waters
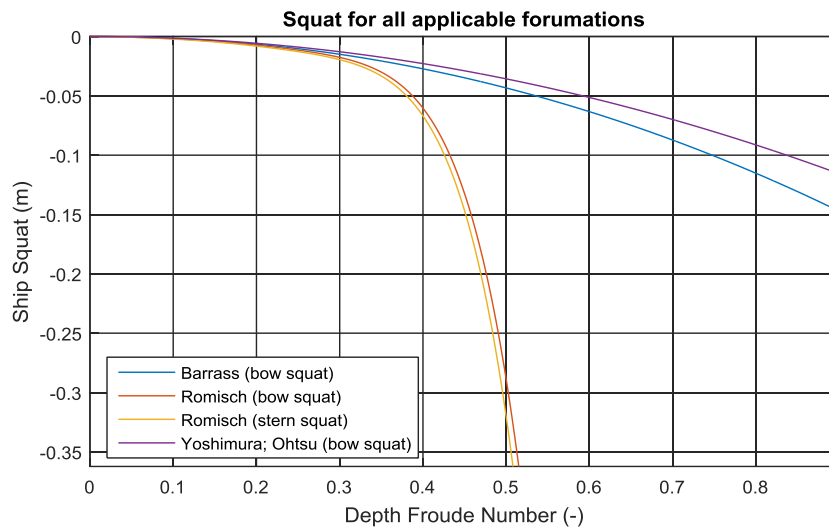
5.1.4 Channel 4

Figure 15. In-house code output: Empirical formulae for channel 4

For this configuration, the theory developed by Tuck (1967) for restricted waters was employed by Slenderflow to produce the midship sinkage and trim, as shown in

Figure **16** and Figure 17, respectively. As mentioned in the Background section, the Slender-Body theory is well suited for wide canals or open shallow waters at low speeds. However, the theory developed by Tuck (1967) seems to provide a good approximation to the CDF results throughout the majority of the range investigated, especially in the low speed range. As observed previously, the difference between the two sets of data increases as we progress through the velocity scale. Finally, the Slender-Body theory does not seem to predict the sharp decrease in sinkage at $F_0 = 0.7$. As the velocity is increased past this point, the vessel's CoG seems to rise out of the water, while the trim increases massively (Figure 17).
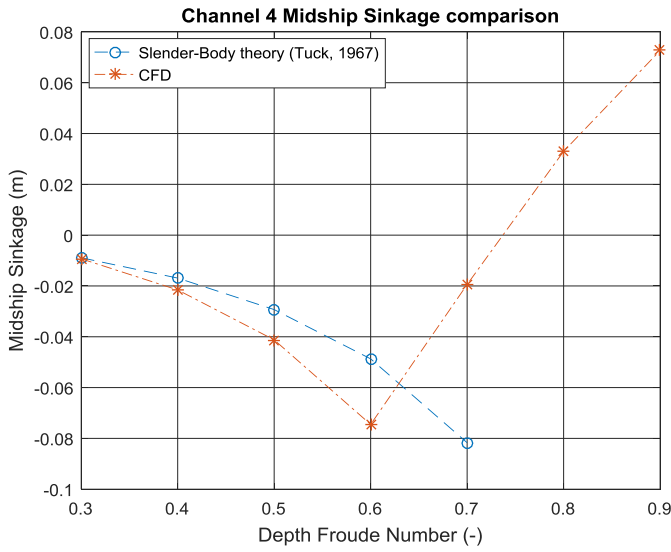

Figure 16. CFD and Slender-Body theory comparison for channel 4
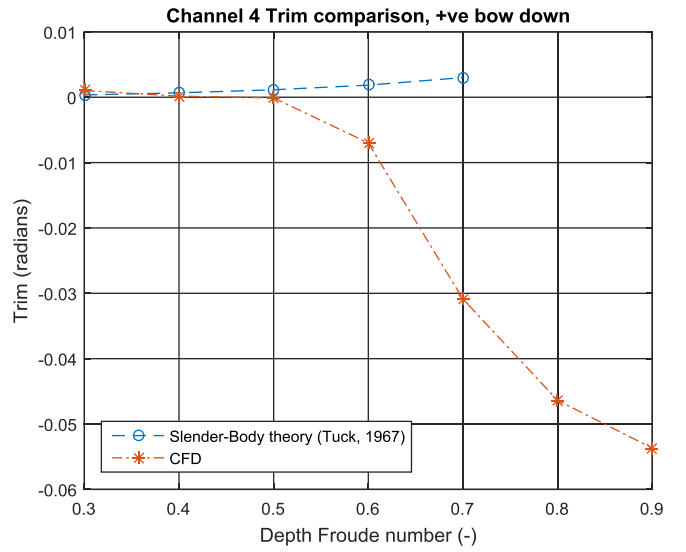

Figure 17. Dynamic trim comparison for channel 4; positive bow down

The trim results predicted by the Slender-Body theory seem to be in best agreement with the CFD results for low speeds, when compared to the previous case-studies. However, the numerical output of Slenderflow does not predict the sharp changes in trim as we move past $F_0 = 0.6$.

5.2 Resistance coefficients

To assess the performance of a vessel, one of the key parameters designers and operators are interested in is the resistance characteristics. The resistance of a ship can be broken down into several components. More specifically, frictional resistance (R_F) and pressure resistance (R_P), which can be further decomposed into wave making resistance (R_W) and viscous resistance (R_V). For the purposes of this paper, R_V and R_W are presented jointly as R_P. Then, the total resistance (R_T) is defined as shown as the sum of R_W and R_P. A more convenient way of presenting the resistance is in non-dimensional coefficient form. To achieve this, each component described above is divided by $0.5\rho S_w V^2$, where S_w is the ship's wetted area. In this form, the performance of a ship can more easily be compared to other vessels.

To begin with, the resistance coefficients calculated using CFD are given for all configurations in Table 2. To put the shallow water region in perspective, in the table the F_∞ distribution of values is added where relevant.

Table 2. Resistance coefficients ($\times 10^{-3}$) obtained using CFD

	F_0	0.3	0.4	0.5	0.6	0.7	0.8	0.9
	C_P	1.616	1.791	1.758	3.108	3.178	8.645	21.722
Channel 1	C_F	3.519	3.456	3.354	3.439	3.447	3.846	3.589
	C_T	5.134	5.247	5.112	6.198	6.625	12.491	25.311
	F_∞	0.522	0.696	0.870	1.044	1.219	1.393	1.567
	C_P	10.508	9.327	10.234	21.384	26.089	24.161	25.873
Channel 2	C_F	5.123	4.727	4.793	4.541	3.689	3.222	3.330
	C_T	15.631	14.054	15.027	25.925	29.778	27.383	29.204
	F_∞	0.369	0.492	0.615	0.739	0.862	0.985	1.108
	C_P	2.910	2.545	2.735	2.988	8.630	24.421	26.691
Channel 3	C_F	3.527	3.453	3.373	3.455	4.025	3.618	3.383
	C_T	6.437	5.998	6.109	6.443	12.655	28.039	30.073
	C_P	5.349	9.906	10.700	26.074	54.230	59.650	55.186
Channel 4	C_F	4.331	4.505	4.611	5.563	5.751	5.120	4.558
	C_T	9.680	14.411	15.312	31.637	59.980	64.770	59.744

Of particular interest are the values of the total resistance coefficient, because they show the overall performance of the ship. Beck et al. (1975) briefly discuss the effect of depth change of the exterior shallow water region and concludes that as h_∞ increases, resistance decreases. This statement is validated by the CFD results, but perhaps more importantly, this proves the assertion that the exterior region's depth has a significant impact on the resistance of a ship. Since the Slender-Body theory is linear, it is incapable of calculating the resistance, which is non-linear. The total resistance coefficients are shown in Figure 18, which presents highly interesting results. Namely, there is a dramatic difference in ship behaviour between case-studies. As reported in Castiglione et al. (2014), C_T shows higher peaks and increases in magnitude as the water depth decreases, which our CFD results verify. For the case-studies incorporated here, it is shown that not only the depth, but width and channel cross-section are highly influential on the magnitude and peak of the resistance coefficient.

 Figure 19 shows the sinkage distribution for all case-studies obtained using CFD. Several important conclusions can be drawn by comparing the sinkage curve of channels 2 and 4. As stated in Beck et al. (1975), modelling a canal case-study is equivalent to modelling one where the exterior water region has attained the critical value ($F_\infty = 1$), provided the width for both is the same. Examining the 'cusp' of each curve we note that for the two channels in question it is located at $F_0 = 0.6$.

For each channel, the cusp of the sinkage curve is a direct indication of where along the velocity scale the relative importance of sinkage and trim reverse. As the channel cross-section becomes more constrained, the cusp is located earlier. This suggests that reducing the channel cross-section, whether vertically or laterally, has a pronounced influence on the behavior and performance of a ship.
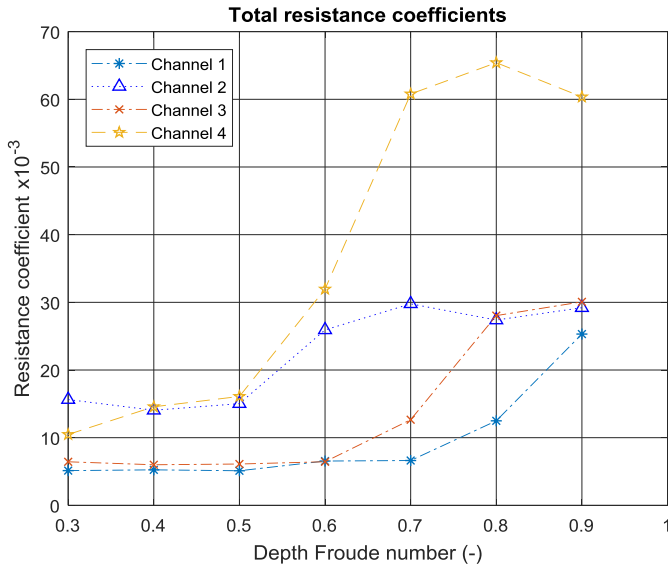
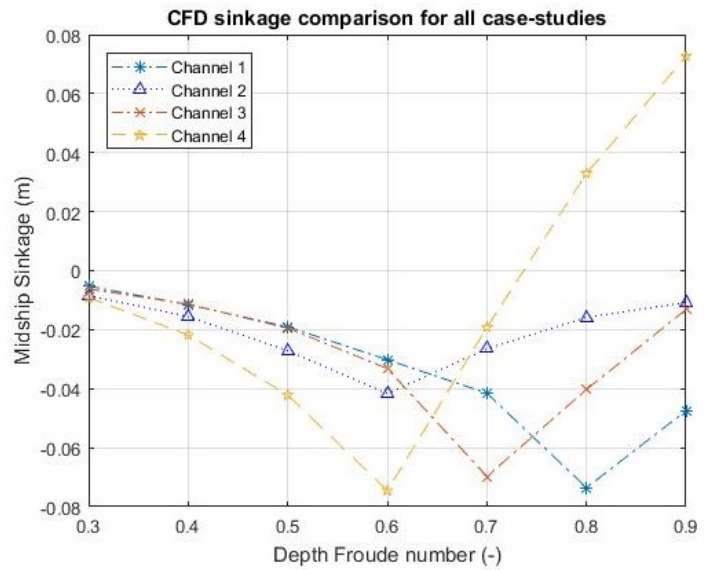**Figure 18.** Total resistance coefficients for the four different channel configurations obtained using CFD.

Figure 19. CFD sinkage comparison for all case studies

6. Concluding remarks

As part of this study, empirical, analytical and unsteady RANS methods were employed to predict the sinkage, trim and resistance of the DTC advancing through a variety of channels at a wide range of speeds. Two dredged channels of varying exterior depth were modelled in order to quantify the effect of the step on ship behaviour and performance. A canal case-study was also adopted to show the restricted width effects on the parameters of interest.

The results show good agreement between empirical formulae, Slender-Body theory and CFD in the low speed range. As we move up the velocity scale, some disagreement is present between the Slender-Body theory and CFD results, attributable to the neglect of viscous and non-linear terms by the Slender-Body theory.

The assertion that sinkage is important in the low speed range, whereas trim is the leading factor in the high-speed range was shown to hold for all case-studies. Resistance was also revealed to be highly sensitive to changes in the underwater topography of the channel.

The hypothesis of Beck et al. (1975), according to whom the resistance of a ship decreases as the exterior depth (h_∞) increases in a dredged channel, was proven via our CFD results. Furthermore, the components of the total resistance were shown to vary dramatically between the case-studies.

This paper has provided a strong basis from which further investigations into the behaviour and performance of ships in shallow water can benefit.

Acknowledgement

this paper is openly available from the University of Strathclyde data repository at http://dx.doi.org/10.15129/b094fbee-cfd4-4ed8-b2cc-551108c67d70. It should be reported that the extended version of this paper has been published in the Journal of Fluids and Structures (https://www.sciencedirect.com/science/article/pii/S0889974617303924).

7. References

BARRASS, C. 2012. Ship squat in open water and in confined channels-Chapter 17.

BECK, R. F., NEWMAN, J. N. & TUCK, E. O. 1975. Hydrodynamic forces on ships in dredged channels. *Journal of Ship Research*, 19(3), 166-171.

BRIGGS, M. J. 2006. Ship squat predictions for ship/tow simulator. DTIC Document.

BRIGGS, M. J. 2009. Ankudinov Ship Squat Predictions-Part 1: Theory, Parameters, and FORTRAN Programs. DTIC Document.

CD-ADAPCO 2016. Star-CCM+ User Guide 11.02. USA.

CASTIGLIONE, T., HE, W., STERN, F. & BOVA, S. 2014. URANS Simulations of Catamaran Interference in Shallow Water. *Journal of Marine Science and Technology*, 19(1), 33-51. https://doi.org/10.1007/s00773-013-0230-5.

DEBAILLON, P. 2010. Numerical investigation to predict ship squat. *Journal of Ship Research,* 54**,** 133-140.

GOURLAY, T. 2008. Slender-body methods for predicting ship squat. *Ocean Engineering,* 35, 191-200.

GOURLAY, T. P., HA, J. H., MUCHA, P. & ULICZKA, K. 2015. Sinkage and trim of modern container ships in shallow water. 22nd Australasian Coastal and Ocean Engineering Conference and the 15th Australasian Port and Harbour Conference, 2015. Engineers Australia and IPENZ, 344.

HA, J. H. & GOURLAY, T. P. 2017. Validation of container ship squat modelling using full-scale trials at the Port of Fremantle. Accepted, to appear in *Journal of Waterway, Port, Coastal and Ocean Engineering*.

HAVELOCK, T. H. 1908. The propagation of groups of waves in dispersive media, with application to waves on water produced by a travelling disturbance. *Proceedings of the Royal Society of London. Series A, Containing Papers of a Mathematical and Physical Character,* 81, 398-430.

ITTC 2011. Practical Guidelines for Ship CFD Applications. ITTC.

JACHOWSKI, J. 2008. Assessment of ship squat in shallow water using CFD. *Archives of Civil and Mechanical Engineering,* 8, 27-36.

MICHELL, J. H. 1898. XI. The wave-resistance of a ship. *The London, Edinburgh, and Dublin Philosophical Magazine and Journal of Science,* 45**,** 106-123.

EL MOCTAR, O. E., SHIGUNOV, V. & ZORN, T. 2012. Duisburg Test Case: Post-panamax container ship for benchmarking. *Ship Technology Research,* 59**,** 50-64.

MUCHA, P. & EL MOCTAR, O. E. 2014. Numerical prediction of resistance and squat for a containership on shallow water. 17th Numerical Towing Tank Symposium, Marstrand, Sweden, September 2014.

MUCHA, P., EL MOCTAR, O. E. & BOTTNER, C. U. 2014. Technical note: PreSquat - Workshop on numerical prediction of ship squat in restricted waters. *Ship Technology Research: Schiffstechnik*, 61(3), 162-165.

ULICZKA, K. 2010. Fahrdynamisches verhalten eines groben containerschiffs in seiten- und tiefenbegrenztem fahrwasser. Bundesanstalt für Wasserbau, Hamburg.

PIANC 1997. Approach Channels A Guide for Design. *Final report, PIANC Bulletin,* 95.

TEZDOGAN, T., DEMIREL, Y. K., KELLETT, P., KHORASANCHI, M., INCECIK, A. & TURAN, O. 2015. Full-scale unsteady RANS CFD simulations of ship behaviour and performance in head seas due to slow steaming. *Ocean Engineering,* 97, 186-206.

TEZDOGAN, T., INCECIK, A. & TURAN, O. 2016. A numerical investigation of the squat and resistance of ships advancing through a canal using CFD. *Journal of Marine Science and Technology,* 21, 86-101.

TUCK, E. 1966. Shallow-water flows past slender bodies. *Journal of fluid mechanics,* 26**,** 81-95.

TUCK, E. 1967. Sinkage and trim in shallow water of finite width. *Schiffstechnik,* 14.

WORTLEY, S. 2013. CFD analysis of container ship sinkage, trim and resistance. *B. Eng mechanical engineering project report*.